CHAPTER II

EXPERIMENTAL TECHNIQUES

The results described in this thesis have been obtained using different experimental techniques, viz., Xray diffraction, high pressure and miscibility methods. The details of the Xray and pressure set ups are discussed in this chapter while those concerning miscibility technique are discussed in chapter III.

2.1 XRAY DIFFRACTION

Two types of Xray diffraction systems are used depending upon the requirement. For low resolution experiments and in particular where the complete picture in reciprocal space was necessary, the photographic technique was used. All the high resolution studies were carried out using a computer controlled Guinier diffractometer. These two types of apparatus will be described separately in the following.

2.1.1. Diffractometer Set Up

Fig.2.1 shows a schematic view of the scattering geometry used in the experiments.

a) Source and Detector

A conventional Xray Generator (Enraf Nonius, Model 583) with

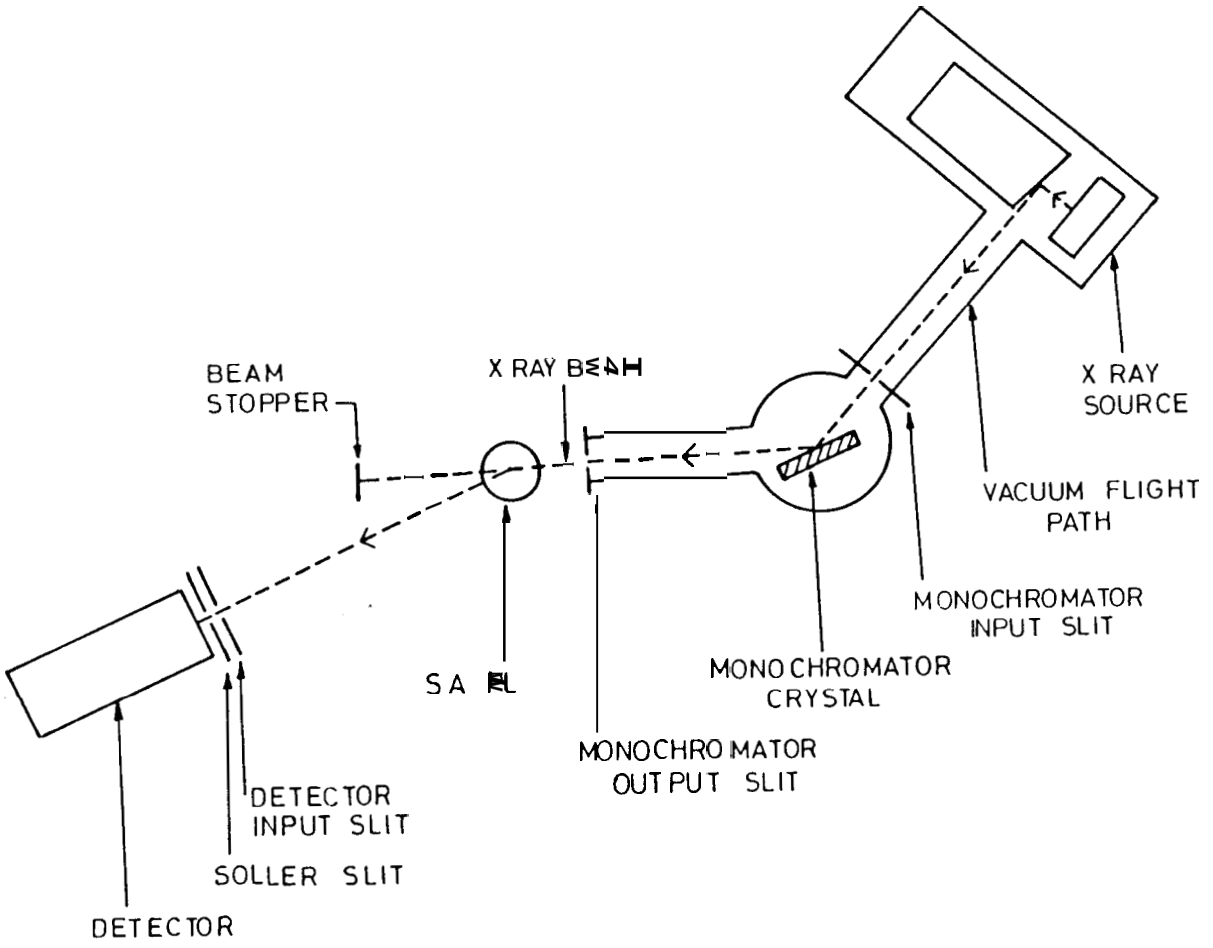

FIGURE 2.1

Top view of the experimental set up

a fine focus tube (Phillips PW2213/20, copper target) was used. The tube was generally operated at 50 KV and 26 mA. The beam from the Xray tube enters the monochromator after passing through a short vacuum path. The monochromator input slits were kept wide open to avoid spurious trimming of the incoming beam. A bent quartz crystal monochromator cut for $(10\bar{1}1)$ reflections was used in the Johansson geometry. The crystal is oriented to select the characteristic CuK_α radiations ($\lambda = 1.54051$ Å). The monochromator slits are further trimmed to eliminate the K_{α_2} rays so that highly monochromatic K_{α_1} rays emerge from the output slit of the monochromator. These rays, if unhindered, get focussed on the circumference of the Guinier circle. The detector, viz., a scintillation counter (Bicron) lies on the circumference of the Guinier circle for asymmetric transmission mode. A platinum edged slit, which was razor sharp to eliminate any shadow effects, was used to control the width of the beam falling on the counter. The vertical divergence of the scattered beam was controlled by a pair of Soller slits located in front of the detector mounted on an arm which moves along the Guinier circle. This arm was driven by a stepper motor with an angular resolution of 0.001 of a degree. It is extremely important to ensure that the direct beam does not hit the detector. This was achieved by a beam stopper positioned suitably.

b) Sample Holder and Heater Design

Fig.2.2 shows the schematic diagram of the sample holder. It consists of a copper rod with a narrow capillary bore drilled along the axis from the top end to house the Lindemann capillary which contains liquid crystal samples. (The bore is about 0.6 mm in diameter and 20 mm long.) A pair of slots are cut on the rod along the length diametrically opposite to each other. These slots serve as the entrance and exit slits for the Xray beam. One of these slots with its edges tapered to give an angle of 20° at the axis of the cylinder is referred to as exit slit of the sample holder. The stem at the lower end helps in fixing the sample holder on to the goniorneter base.

A sectional view of the heater (oven) used to heat or cool liquid crystal samples is given in Fig.2.3. Essentially, it has a thick copper rod having a cavity cut along the axis to house the sample holder. This sample cavity dimensions are so chosen that the sample holder fitted exactly into it. Two vertical slots cut on the cylinder serve as the entrance and exit slits (windows) for the Xray beam. A hole drilled along the axis of the copper rod from the top end houses one of the junctions of a chromel-alumel thermocouple sheathed in a ceramic tube. The tip of the junction sits in the close proximity of the sample (in the sample holder) and is fixed firmly with an adhesive. The temperature of the sample is varied by regulating the current passed through a thermofoil (MINCO) heater wrapped around the

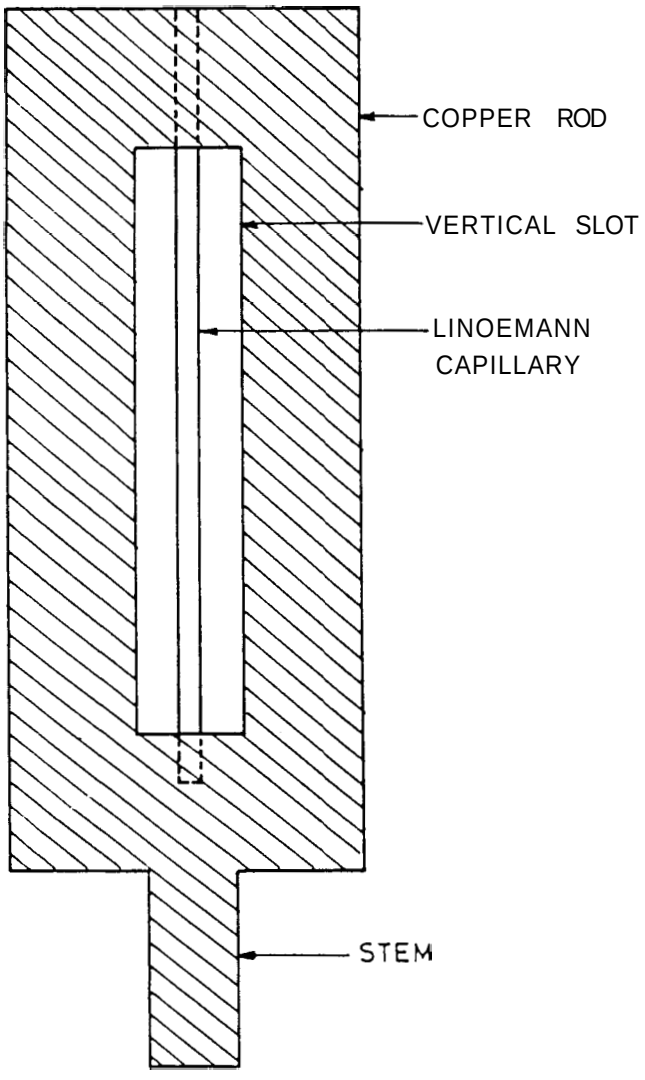

Figure 2.2

Schematic diagram of the sample holder

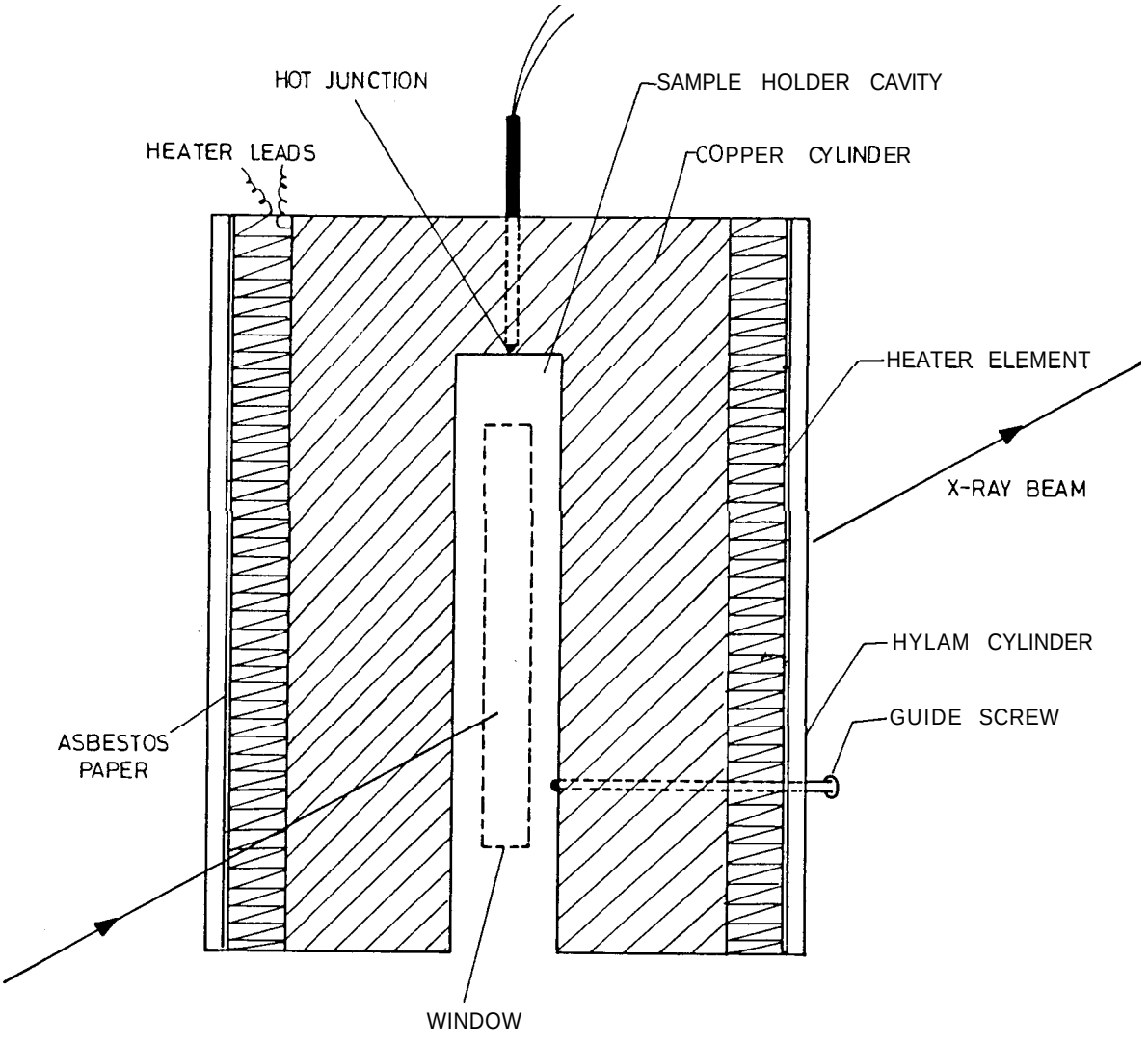

Figure 2.3

Schematic diagram of the heater assembly

copper rod. The thermofoil is surrounded by a layer of asbestos paper and then by a thermally insulating hylam cylinder. This combination serves to reduce the heat loss due to radiation. The windows on the cylinder are covered by thin mylar sheets to prevent the air currents which can be detrimental to the temperature stability of the sample. A guiding screw threading through the body of the heater helps in holding the sample holder firmly with respect to the heater. Care is taken to see that the windows on the heater body are aligned properly with respect to the slits of the sample holder and also that the tapered slot on the sample holder is directed towards the detector. This ensures that the Xray beam scattered by the sample reaches the detector without any hindrance. The material of the oven as well as the sample holder is copper. The temperature uniformity across the illuminated portion of the sample holder is better than 5 mK. This is evident from the Xray data which show sharp phase transitions to within a few mK. The Xray set up and the oven are housed in a chamber covered by thermal insulating sheets.

c) Temperature Calibration

Most of our Xray scattering experiments required the measurement of temperature of the sample to a high degree of accuracy. For this the hot junction of the thermocouple is calibrated to give the correct temperature of the sample. Several compounds of high purity and with very sharp mesophase-mesophase transitions were chosen. The

Block diagram of the experimental set up used is shown in Fig.2.4. Light from a He-Ne laser (Spectraphysics 5 mW) was made to fall on the sample loaded into the Lindemann capillary. The sample is cooled slowly at 1-2°C/hour. The photodetector system collects the light transmitted by the sample. The voltage drop across a fixed resistance of 1 Kiloohm caused by the current output of the detector was measured using a digital multimeter. A parallel connection from this was taken to one of the channels of a multichannel recorder (Linseis, Model 2041) through a low voltage source. Using this source as an off-set control, small intensity changes over and above a large background intensity could be easily monitored. The temperature of the sample was measured using a thermocouple in conjunction with a programmable digital nanovoltmeter (Keithley 181). The voltage output of the thermocouple (thermo emf) was fed to another channel of the multichannel recorder. Thus both intensity and temperature could be simultaneously monitored and recorded. The temperature corresponding to the abrupt change in intensity on the scan is taken as the transition temperature (in mV). The transition temperatures (in mV) for various mesophase-mesophase transitions were obtained for different compounds measured as described above and these data are listed in Table 2.1. Also listed in this table are the transition temperatures for the same materials as determined using a polarising microscope fitted with a programmable hot stage (Mettler FP52/FP800). The plot of transition temperatures measured in the Xray set up

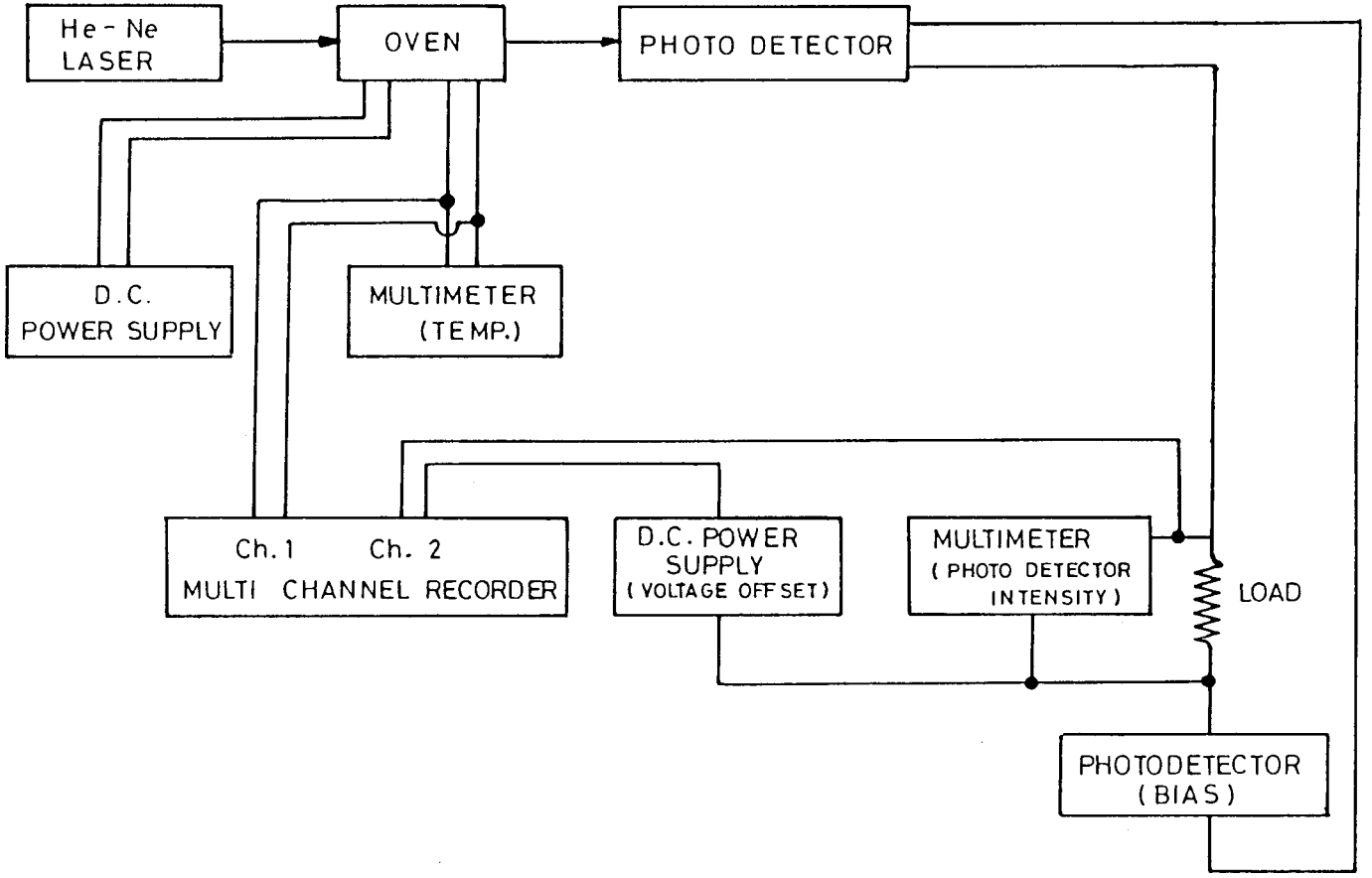

Figure 2.4

Schematic diagram of experimental set up used for thermocouple calibration

TABLE 2.1

Materials used for the temperature calibration of the thermocouple (of Xray set up) and their transition temperatures measured by using the Mettler hot stage. The corresponding e.m.f. of the thermocouple are also given

Compound	Transition temperature as observed (in °C) by Mettler hot stage	Thermo e.m.f. (in mV) at transition measured using the optical transmission method
4'-n-Octyloxy-4-cyanobiphenyl (8OCB)	40.57 - 40.52 (40.545)	1.569
	80.6 - 80.52 80.56	3.207
4'-n-Cyanobenzylidene-4-octyloxy-aniline (CBOOA)	107.63	4.358
p-Dohexyloxy azoxy benzene (HOAB)	124.55	5.060
p-Azoxyanisole (PAA)	135.89	5.530
p-Azoxyphenetole (PAP)	167.76	6.865
p-Anisaldazine	183.79	7.512
4-n-Butoxybenzylidene-4'-n-propoxy aniline	113.59	4.702

(V, in mV) versus the transition temperatures as measured using the Mettler hot stage (T, in °C) is shown in Fig.2.5. These data were fitted to a second degree polynomial, $T = a_0 + a_1 V + a_2 V^2$ using a least square program. The constants of the fit are, $a_0 = 2.9095$, $a_1 = 23.9586$ and $a_2 = 0.0\,166$.

d) Measuring Electronics and Data Collection

The electronic control of the diffractometer is provided by a HP86B computer with 128 Kbytes physical memory. The temperature is measured by a Keithley digital nanovoltmeter (Keithly 181). All the instruments are interfaced to the computer by using either Hewlett-Packard Interface Bus or an IEEE-488 card. Pulses from the detector after being fed through the amplifier and descriminator reach the ratemeter (Scalar) where the intensity of the Xray beam is expressed as counts per second. The descriminated pulse output is fed to a stepper motor control (SMC) which also monitors the position of the detector. The data collection is done by an elaborate program. This program controls counting, duration of counting time, driving of stepper motor, data storage and data analysis.

e) A Typical Experiment

The block diagram of the experimental set up used is shown in Fig.2.6. The liquid crystal sample is filled into a Lindemann capillary tube in the molten phase using a microsyringe with a fine control

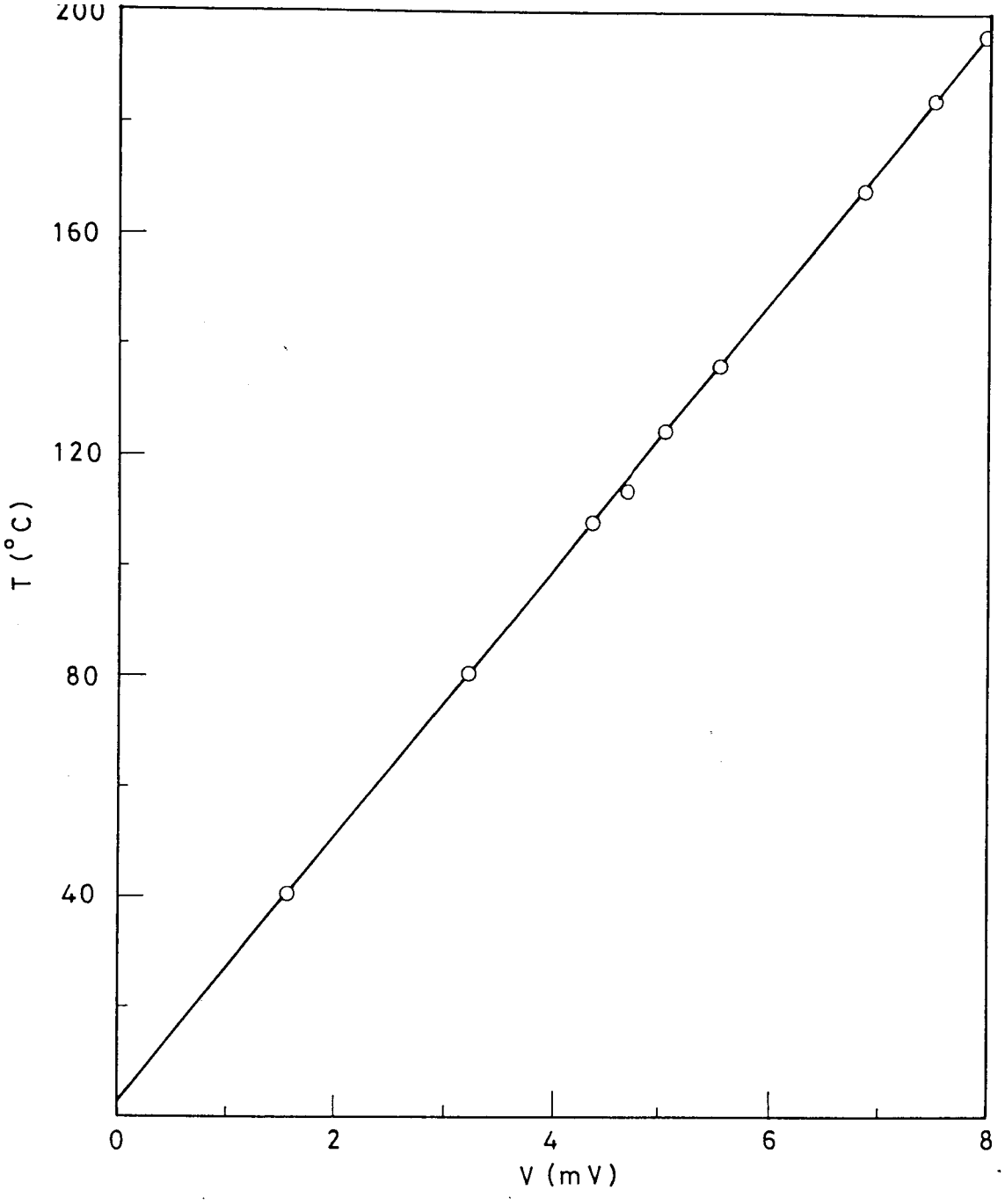

Figure 2.5

Temperature calibration curve of the thermocouple. T is the temperature in °C as measured optically using a hot-stage and V the thermo e.m.f. in mV corresponding to the phase transition. These data were fitted to a polynomial to obtain the calibration constants as described in the text.

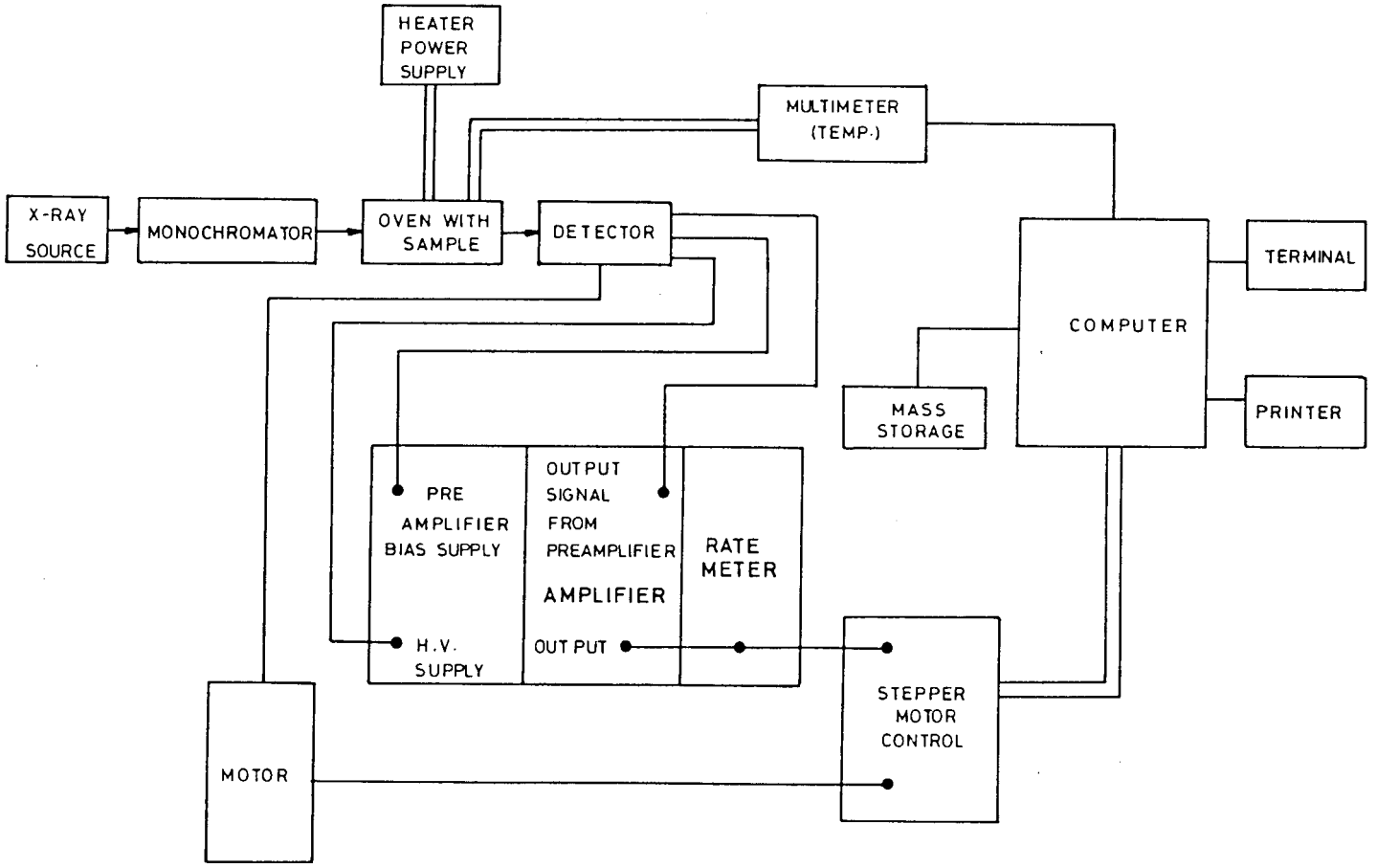

Figure 2.6. Block diagram showing the experimental set up used for Xray diffraction studies.

attachment. After taking the sample into the capillary, the capillary is cut into a length of 15–17 mm (sample length –10 mm) leaving sufficient gaps on either side of the sample. The capillary was then truncated and sealed on both ends using a thin flame. It was ensured that the sample was not overheated in this process. Any excessive heating resulted in a marked darkening of the sample. In such a case, the capillary was discarded and a fresh sample was mounted again. The capillary is then mounted carefully in the sample holder so that even on gently tapping the sample body, the capillary remained vertical in position (along the axis of the cylinder). The sample holder (with the capillary) is then pushed into the cavity of the oven. After ascertaining that the two vertical slits on the sample holder were properly aligned with reference to the entrance and exit windows of the heater, the sample holder is fixed firmly to the oven with the help of the guiding screw. The sample was then heated initially to the nematic phase and then cooled very slowly (1-2°C/hr.) in the presence of a magnetic field (Bruker Electromagnet, B-E 25) of strength 2.4 Tesla. This resulted in an extremely well aligned sample. Having thus obtained a well oriented smectic A phase, the sample along with the temperature controlled oven was transferred on to the goniometer head of the diffractometer. The position of the oven on the goniometer is carefully adjusted to ensure that the monochromator exit slit, the entrance and exit windows of the oven are collinear. An initial scan was taken (along the equatorial plane) by changing the position of

the counter in steps of 0.01" and the approximate position (θ) of the diffraction peak was obtained. A refined θ scan was then taken around this θ position by moving the counter in steps of 0.001". The data were fitted to a second degree polynomial by using least-squares-fit program. The value of θ obtained in this manner was corrected (discussed in the next sub-section) and used in the calculation of layer spacing [$d = \lambda/(2\sin\theta)$]. The on-line θ refinement at any temperature required about 5 minutes. During this period the temperature of the sample was maintained to a constancy of ± 10 mK or better. A typical initial scan and refine θ scan are shown in Figs. 2.7a and 2.7b. An on-line hard copy provided the complete information such as temperature, scattering angle, intensity maximum and wavevector related to any scan. The precision of measurement of wavevector is $\sim 2 \times 10^{-4}$ Å^{-1}

f) Wavevector Calibration

It is possible that the layer spacing determined as explained earlier may differ slightly from the standard value (or true value) due to the limitations imposed by the experimental conditions. In order to account for this we measured the scattering angle for a set of compounds exhibiting smectic A phases for which the layer spacings were known, exactly under the same conditions as those under which a normal experiment is done.. From the knowledge of the deviation of each measured scattering angle ($\Delta\theta = \theta' - \theta$) from the

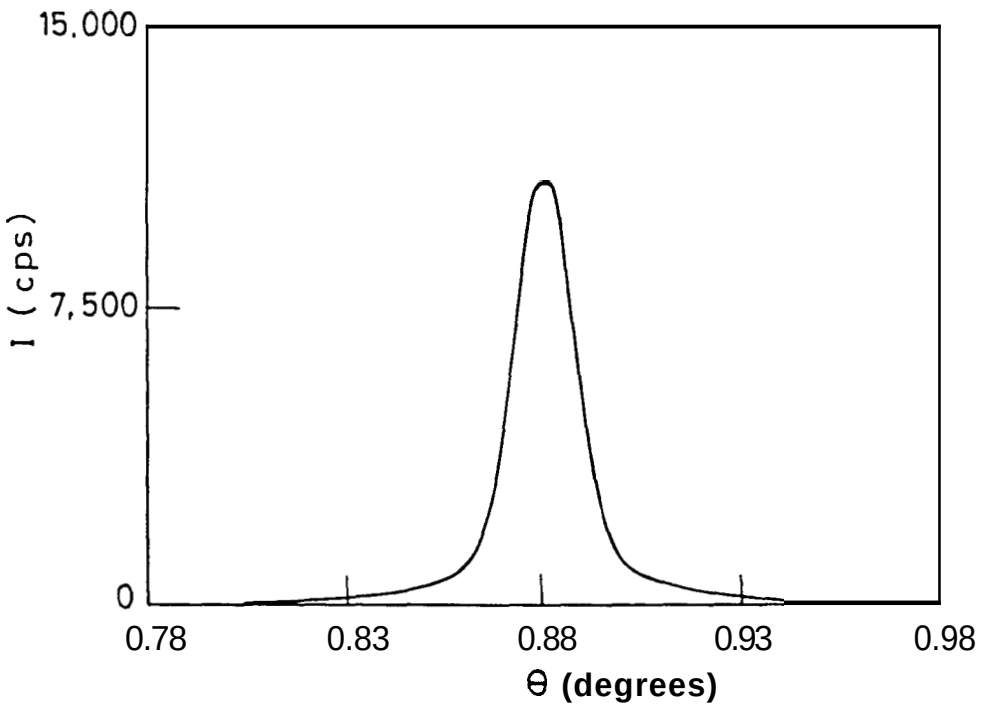

Figure 2.7(a)

Initial intensity scan (I-θ) showing the intensity of the scattered beam as a function of scattering angle.

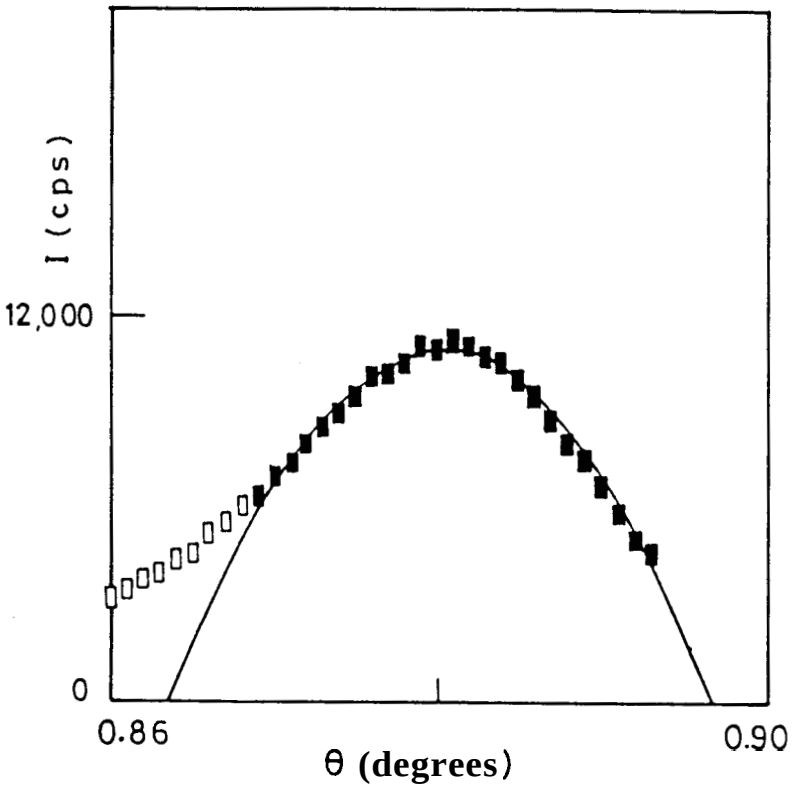

FIGURE 2.7(b)

Refine I-θ scan. Rectangles are the data and the solid line is a computer fit of the data to the equation of a parabola.

standard value (θ'), the correction to the measured θ was determined from the standard interpolation technique. The materials chosen for calibration, the standard θ' from known layer spacings[1,2] and the scattering angle θ measured from the experiment are listed in Table 2.2.

g) Wavevector Resolution

The line shape observed in an Xray scattering experiment is given by the convolution of the structure factor and the spectrometer resolution function. The latter includes broadening of the peak due to slit width, sample size and the Darwin width of the monchromator crystal. In our experiments the resolution of the instrument is also influenced very much by the sample mosaicity. Even at the smallest slit width permitted by the set up (10 μ) an I-θ scan (intensity-scattering angle) shows a peak with half width at half maximum of —0.01".

The wavevector spread (dq) in the equatorial direction due to this angular width $d\theta \sim 0.01°$ as calculated from the equation

$$dq = \frac{4\pi}{\lambda} \cos\theta \, d\theta$$

for a typical scattering angle of $\sim 0.88°$, is dq = 1.4235 x 10^{-3}/Å. In other words this set up permits us to resolve two peaks whose minimum separation in q space is 1.4×10^{-3}. The precision in the determination of q itself at any temperature is $\pm 2 \times 10^{-4}$ Å^{-1}.

TABLE 22

List of the compounds chosen for wavevector calibration along with the standard values of scattering angles, scattering angles measured and the difference

Compound	Standard θ' (in °)	Measured θ (in °)	$\Delta\theta = \theta' - \theta$
CBOOA q_0'	1.2574'	1.1867	0.0707
DB5 i) q_0	0.8679[2]	0.7974	0.0705
ii) $2q_0$	1.7354[2]	1.6602	0.0752
8OCB q_0'	1.3838[1]	1.3122	0.0716

2.1.2 **Xray Set-up** (With flat film photographic detection technique)

In this section we shall describe the set up used for low resolution Xray diffraction experiments. The sample holder and the heater used to maintain the temperature of the sample at any desired value are shown in Fig.2.8. The heater consists of a circular copper rod having a rectangular slot. In order to facilitate mounting between the pole pieces of a permanent magnet, the central portion of the rod was machined to have a rectangular cross-section. Nichrome tape wound on the bottom and top circular parts was used for heating the sample. A small hole (about 0.6 mm diameter) was drilled at the centre of the rectangular portion for the Xrays to enter. The conical angle of the exit aperture (O_1) was about 45°.

The sample holder consisted of a long rectangular copper strip which fitted exactly into the rectangular slot of the heater. The strip had a hole (O_2) of 0.8 mm diameter along the wider side through which a Lindeman capillary tube containing the sample could be inserted. The strip also had two holes (at right angles to the hole in which the sample capillary is located) one for the entrance of the Xrays and the other (O_3) for the diffracted Xray beam. The hole on the exit side had a large taper so that it permits diffraction cone angle of 45°. Both the entrance and the exit holes of the heater were covered by thin mylar strips to avoid air currents affecting the stability

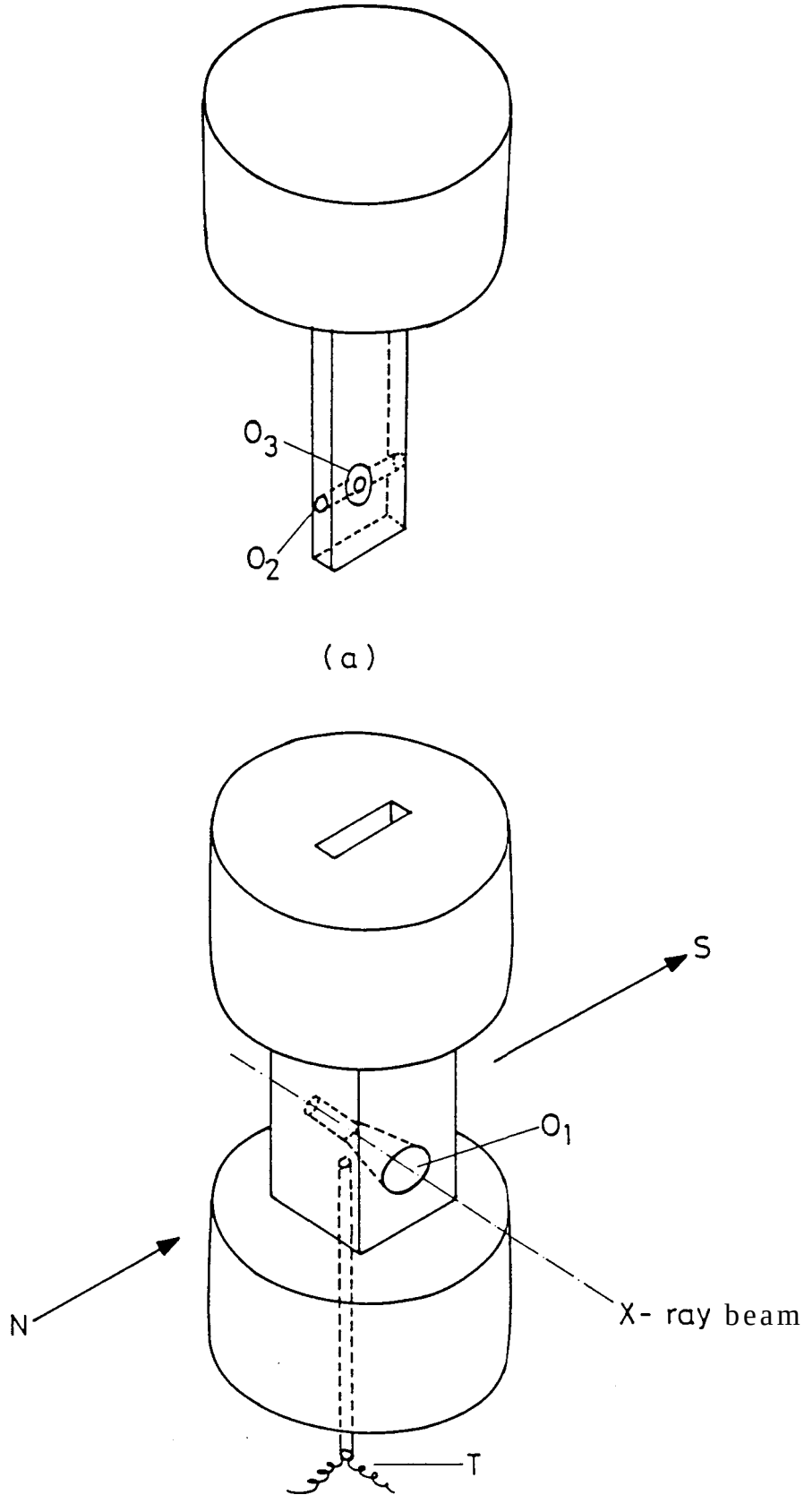

Figure 2.8

Schematic diagram of the sample holder (a) and the heater assembly (b) used for the Xray experiments.

of the sample temperature. The heater was kept between the pole pieces of a permanent magnet of strength 0.4 Tesla such that the sample was positioned at the centre of the pole-pieces and the field was normal to the incident Xray beam. The heater and the magnet assembly were mounted on a stand of adjustable height which also had a provision for precise levelling by means of three secrews.

A copper-constantan thermocouple was inserted into the heater from the bottom such that the junction was as close to the sample as possible. The output of the thermocouple was fed to a digital multimeter. Calibration of the thermocouple was done using standard samples in the manner described in the preceding section.

For Xray studies samples were taken in Lindemann glass capillary tubes and ends of the tubes were sealed in a flame. The tube was mounted in the sample holder and was bathed in monochromatic CuK_{α} X radiation obtained from a Xray generator (Phillips W1730) in conjunction with a bent quartz crystal monochromator (Carl Zeiss Jena). The diffracted Xray beam was recorded on a flat film which was located at the focus of the monochromator. A typical exposure time in the smectic A phase at any temperature was about 10-15 minutes. During this time the temperature of the sample could be maintained constant to within $\pm 0.1^{\circ}C$. After the completion of the experiment, the transition temperature of the sample was remeasured and found to be unaltered within the limits of experimental error

indicating thereby that the sample did not deteriorate during the experiment. The distance between the diffraction spots on the film was measured using a precision comparator (Adam-Hilger Ltd.). The data thus obtained were brought to an absolute scale by using the (100) reflection of p-decanoic acid. The d value of the reflection was taken to be 23.1 Å.[3] The relative accuracy in the determination of d value using this set up was ±0.1°K or better.

2.2 HIGH PRESSURE SET UP

A schematic diagram of the high pressure optical cell[4,5,6] is given in Fig.2.9. The body of the cell (Fig. 2.10) has threaded openings on both sides into which the two plugs (see Fig.2.9) with exactly matching threads can be fitted. On the outside, the plugs have a large tapered opening (70° outside taper) which facilitates a wide viewing angle without affecting the strength of the plug. On the inside, the plugs have small protrusions which are made optically flat by hand-lapping. These plugs keep the sample assembly in position. The central hole of the upper plug is sealed by an optically polished sapphire rod which also forms a part of the sample assembly. The hole in the cell body for the pressure connection consists of two stages: a smaller hole which extends from the interior of the body to about two-thirds of the thickness and joins a larger hole bored from outside. The threads of the plug alone are not enough to hold the plug tightly against the main body of the cell. A thin clearance between the plug

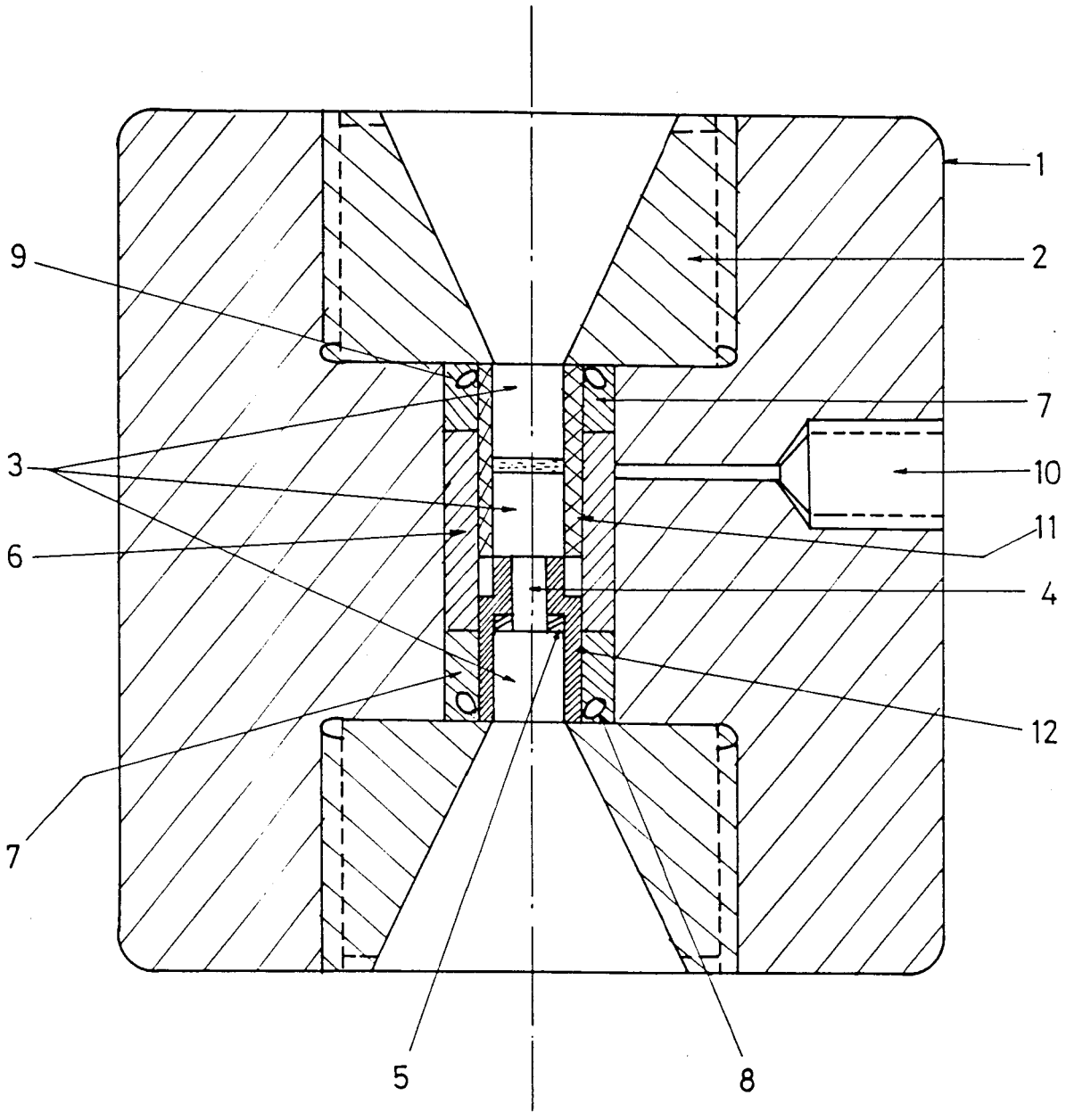

1. CELL BODY 2. STEEL PLUG 3. SAPPHIRE CYLINDERS
4. GLASS ROD 5. WASHER AND SPRING 6. CENTRE SPACER
7. OUTER SPACER 8. 'O' RING 9. ANTIEXTRUSION RING
10. HIGH PRESSURE CONNECTION 11. FLURAN TUBE 12. LOW PRESSURE SEALER

Figure 2.9

HIGH PRESSURE OPTICAL CELL

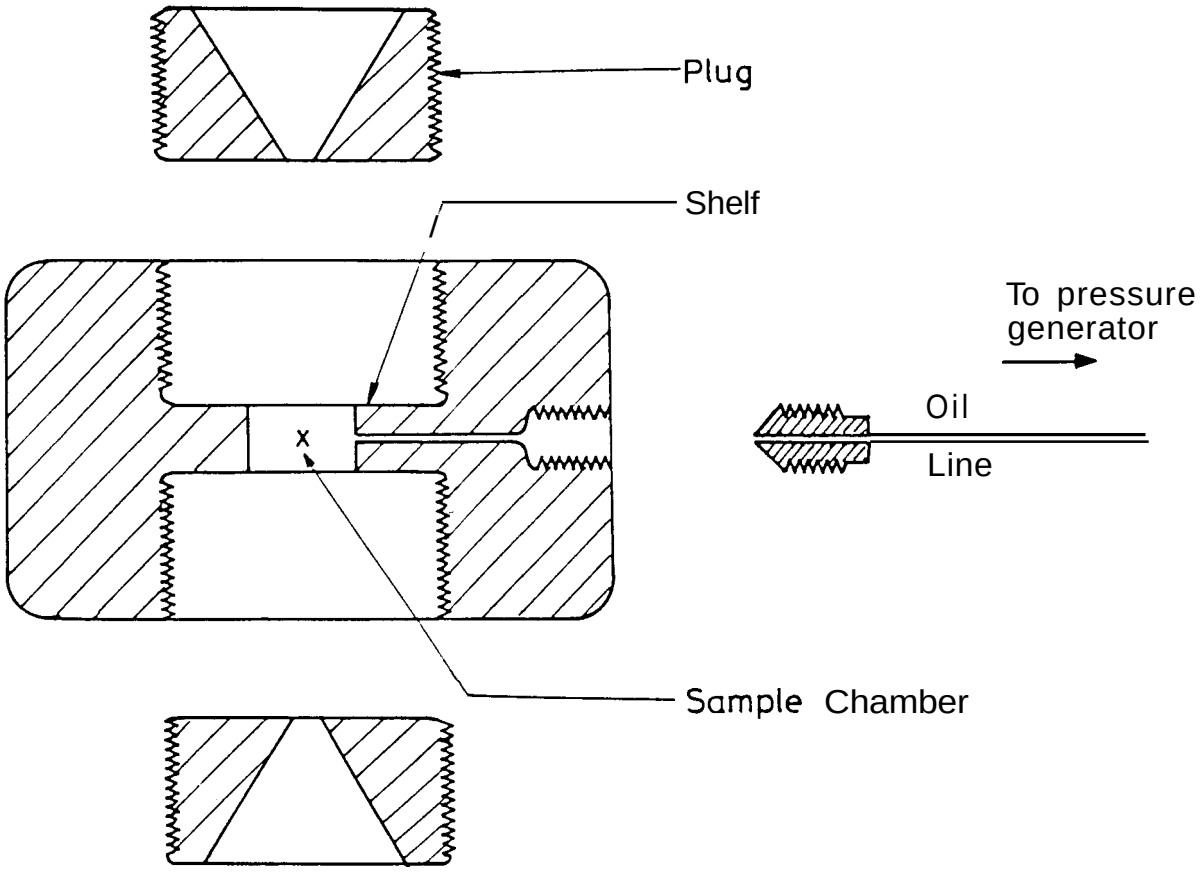

Figure 2.10

Schematic diagram of the basic parts of the high pressure cell.

and the sample chamber caused by a slight lifting of the plug by high pressure leads to a leak of the oil to the outside. This leak is avoided by placing around the junction a neoprene 'O' ring in conjunction with an anti-extrusion ring. The seal at the central hole of the plug is made with optically polished sapphire windows and a small washer made of thin aluminium foil - the washer to fill any crevices on the surface of the plug. The sapphire windows as well as the 'O' ring are held in position initially by the outer.spacer.

Encapsulation of the sample

The sample assembly is schematically represented in Fig.2.11. The sample is sandwiched between two sapphire rods which fit snugly inside a fluran tube. Fluran is an elastomer material which does not react with liquid crystals and at the same time transmits pressure exceedingly well. It can also withstand temperatures up to 270°C. An effective seal is realized by tightly wrapping a thin steel wire around the tubing on the saphhire windows. The inner spacer (low pressure sealer), washer and the spring (see Fig.2.9) centre the bottom sapphire (which is free as it is not used to seal the cap) of the sample assembly and keep it under a light tension. A third sapphire, which is completely isolated from the sample assembly, seals the bottom end of the pressure cell. The space between this third sapphire and the bottom sapphire of the sample assembly is occupied by a glass rod reducing thereby the amount of oil between these two sapphires

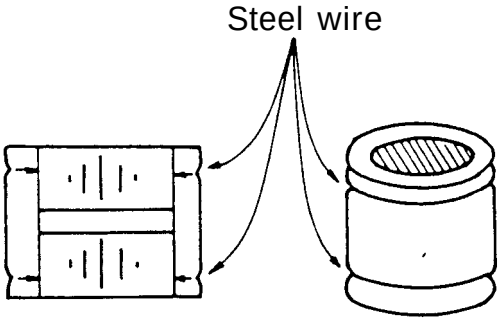

Figure 2.11

Sample Assembly

which otherwise would have decreased the intensity of the transmitted light. It must also be mentioned that all the sapphire rods are specially cut such that the C-axis is perpendicular to the faces and then polished.

Heating and cooling systems

The schematic diagram of the heating and cooling assembly is shown in Fig.2.12. The heating system is made of an aluminium cylinder whose internal diameter is such that the pressure cell could be push-fitted into it. Thus it also acts as a binding ring for the pressure cell. Nichrome tape is wound on mica sheets (which served as electrical insulators) which in turn were wrapped around the inside wall of the aluminium cylinder. The effective heating capacity was about 200 watts. A radial hole was made through the aluminium cylinder to facilitate the taking out of the pressure tubings from the pressure cell to the outside. A Chromel-Alumel thermocouple sheathed in a ceramic tube was used to measure the temperature sensed by the sample. The thermocouple junction is introduced through a small radial hole and is so located that its junction just touches the cell body. No holes are made on the cell body for the insertion of the thermocouple since that would considerably weaken the cell body. There will be however a difference in the temperature of the sample and that sensed by the thermocouple junction. By accurately mapping this gradient at all temperatures, the problem was overcome. These calibration experiments were performed using a uniform heating or

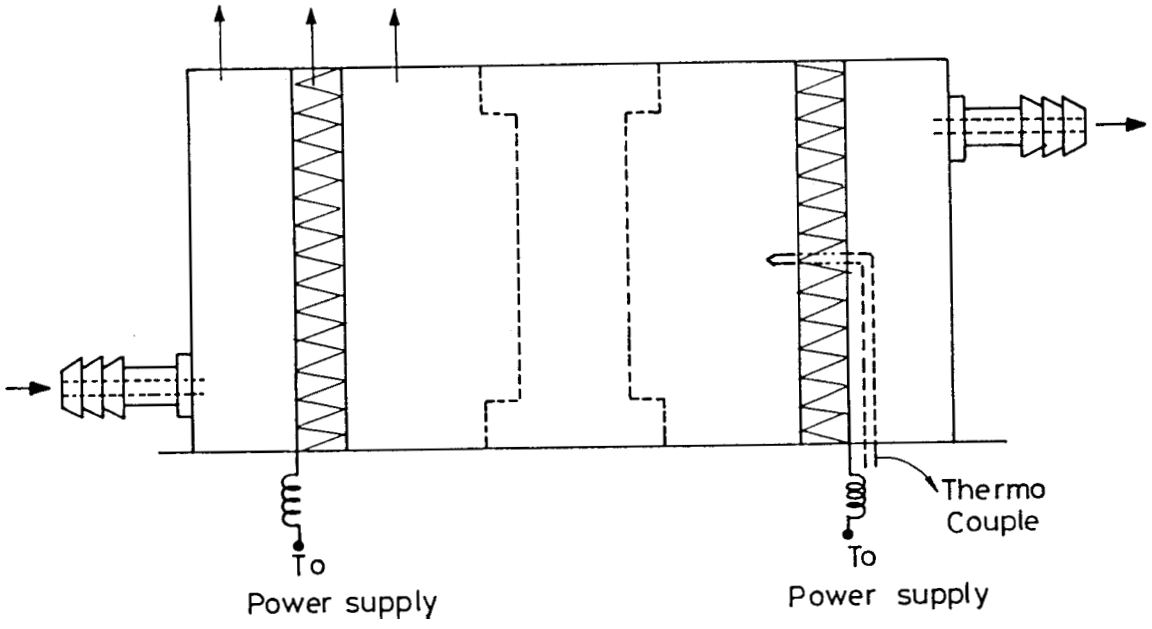

Figure 2.12

Schematic diagram of the heating and cooling assembly

1. High pressure cell, 2. Heater, 3. Cooling unit.

cooling rate of 1°C/min.

The cell was cooled to room temperatures or below using a cooling unit. Above room temperature cooling could be done by merely varying the current through the heating element. A cooling jacket into which the cell can be press-fitted is made using aluminium as the material.By suitably scooping out the inside material from the jacket and by closing the top of the jacket with an aluminium strip, water can be passed into the jacket through a nozzle provided at the ends of the jacket. In fact, the jacket consisted of two 'C' shaped units linked by a hinge. So whenever cooling was necessary it could be slipped through easily. A circulating thermostat was used to pump water (at any desired temperature) into the cooling jacket. The water, as it passes through practically the entire circumference of the cooling jacket, provides a very efficient way of cooling the cell.

High Pressure Plumbing System

The schematic diagram of the high pressure plumbing system used in the present study is shown in Fig.2.13. A hand pump (PPI, USA) is used to generate the pressure in the cell. Fine variations of pressure are achieved by using a pressure generator (HIP, USA) with a small displacement capacity. The line pressure, which is nothing but the pressure experienced by the sample is measured by a Bourdon type (Heise) gauge. The plumbing connections are made through two-way and three-way valves. The advantage of using a three-way valve

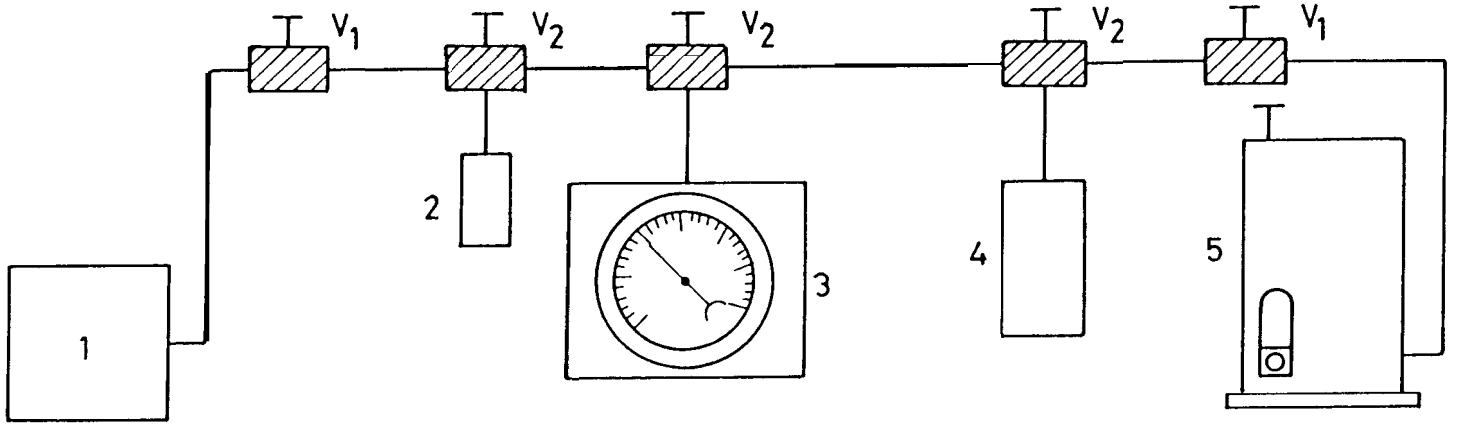

Figure 2.13

Schematic diagram of the high pressure plumbing system

1. High pressure cell
2. Pressure transducer
3. Bourdon gauge
4. Pressure generator
5. Hand pump

V_1 Two-way valve

V_2 Three-way valve.

over that of a T-joint is that the instrument which is connected through the valve can be isolated from the main line when not in use by just closing the valve. The tubing used was made of seamless stainless steel material (ID=2mm and OD=10 mm). The valves as well as the tubing were chosen to withstand line pressures up to 7 kbar.

The sample was pressurised in a fairly straightforward way: the "priming" or initial pressurisation was done using the hand pump. Pulling the handle of the pump up raises the piston and draws oil from the reservoir into the pump's chamber. Pushing the handle down lowers the piston which compresses the oil and sends it through the steel oil line to the cell. After this priming operation pressure could be fine-controlled using the pressure generator.

Determination of the phase transition temperatures

The schematic diagram of the experimental set up used to determine the transition temperatures is shown in Fig.2.14. The transition temperatures were determined as discussed in section 2.1.1 of this chapter.

Temperature calibration of the cell

For the temperature calibration of the cell during the heating and cooling modes, several compounds, non-mesomorphic as well

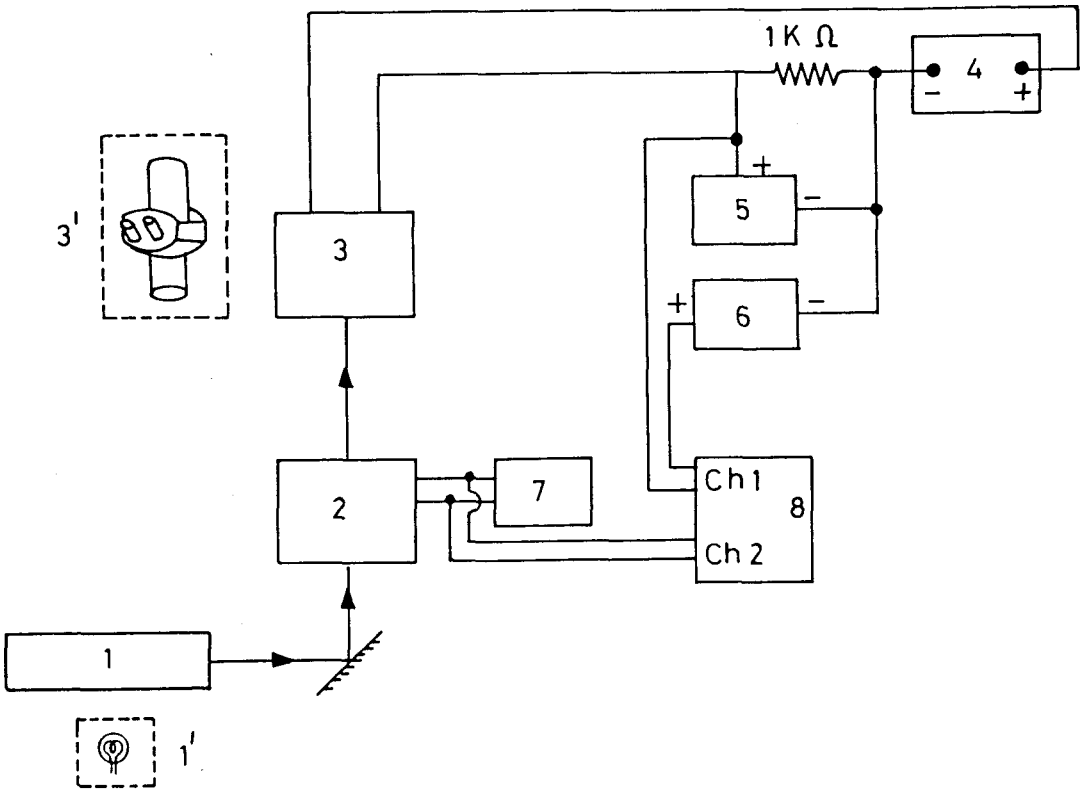

Figure 2.14

Schematic diagram of the experimental set up used for the high pressure experiments.

1. He-Ne laser, 2. High pressure optical cell, 3. Photo detector, 4. Photo detector bias power supply, 5. Multimeter for measuring intensity in terms of voltage, 6. DC standard source used for voltage offset, 7. Multimeter for measuring the thermocouple output, 8. Multichannel recorder.

Instruments indicated by primed numbers are used for microscopic observations.

as mesomorphic, have been used.

a Heating mode. The substances as well as their transition temperatures as measured with the polarising microscope fitted with a programmable hotstage (Mettler FP52/FP800) are listed in Table 2.3. The plot of this temperature against the transition temperatures as measured in our experimental set up is shown in Fig.2.15. The data were fitted to a straight line using a linear least square program. The values of slope and intercept thus obtained are 1.000 and1.571°C respectively.

b Cooling made. As the crystallisation temperature depends upon the rate of cooling, quantity of sample taken, etc. (i.e., degree of supercooling is a function of experimental conditions), the non-mesomorphic compounds cannot be used for the temperature calibration of the cell during the cooling mode. For this purpose, only liquid crystalline transitions which are highly reproducible were used in the cooling mode. The compounds used are listed in Table 2.4 along with their transition temperatures as measured using the Mettler hot stage. The plot of this temperature versus the temperature measured using our set up is shown in Fig.2.16. The values of the slope and the intercept obtained by a linear least square fit of the data to a straight line are 0.985 and -0.269°C respectively.

TABLE 23

Materials used for the temperature calibration of the high pressure cell (heating mode) and their transition temperatures.

Substance	Transition	Actual temperature (°C) (by Mettler)	Observed temperature (°C) (by pressure cell)
CCH_2	Nematic-Isotropic	48.5	51.1
Azobenzol	Solid-Isotropic	67.9	69.2
NPOOB	Nematic-Isotropic	66.2	69.5
CCH_4	Nematic-Isotropic	79.2	80.6
Benzil	Solid-Isotropic	94.7	96.4
7OPDOB	Solid-Smectic C	69.7	71.1
	Smectic A-Nematic	84.1	85.1
	Nematic-Isotropic	87.8	88.8
CBNA	Solid-Smectic A	72.0	73.3
	Smectic A-Nematic	99.3	100.2
	Nematic-Isctropic	105.0	106.1
HOAB	Solid-Smectic C	74.4	75.8
	Smectic C-Nematic	95.0	95.5
	Nematic-Isotropic	124.0	125.7
PAA	Solid-Nematic	118.0	119.9
	Nematic-Isotropic	135.2	137.1
PAP	Solid-Nematic	140.0	141.6
	Nematic-Isotropic	165.2	167.4

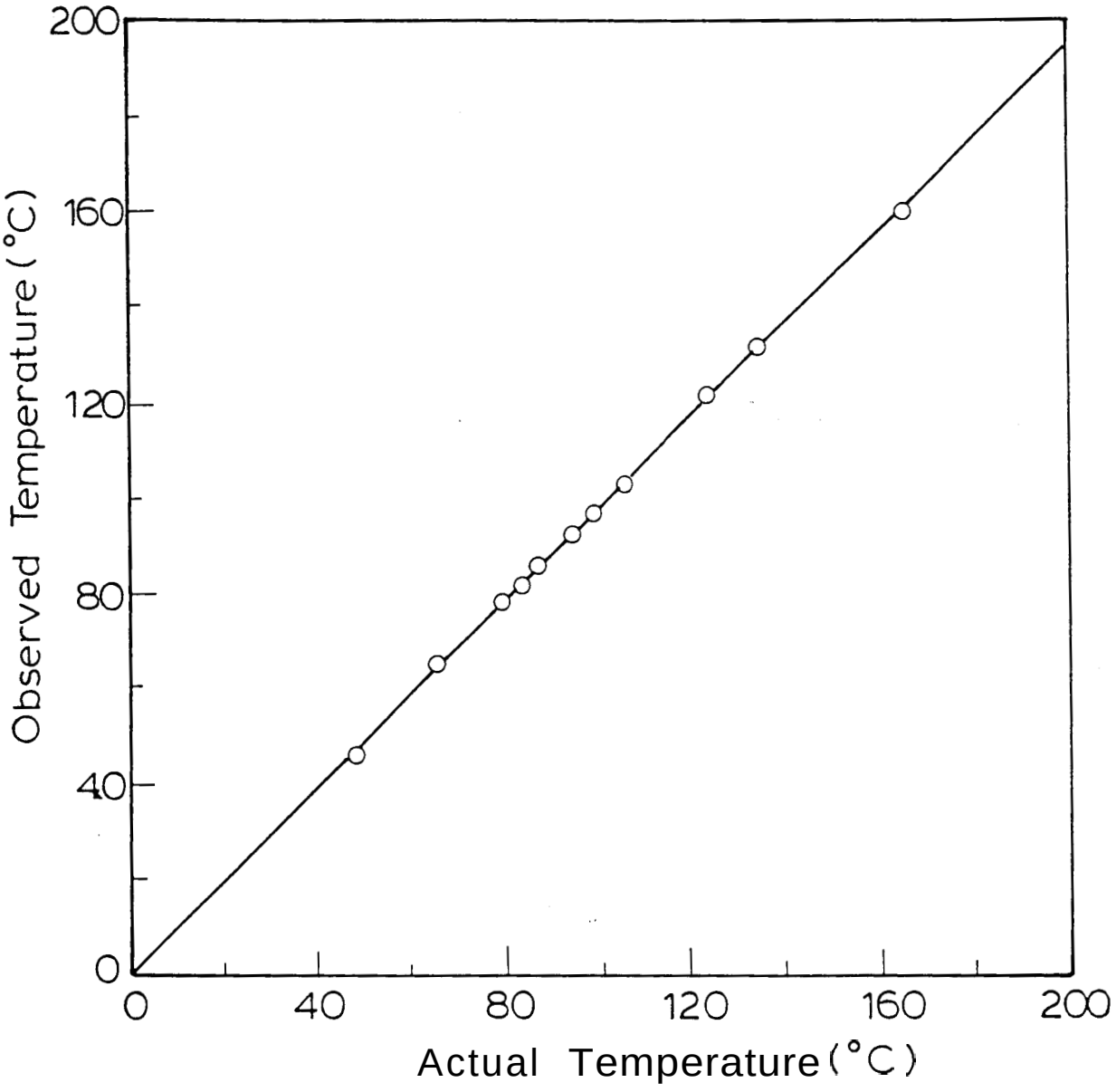

Figure 2.15

Temperature calibration curve of the high pressure cell in the heating mode using the substances listed in Table 2.3.

TABLE 24

Temperature calibration of the high pressure cell during cooling: Materials used and their transition temperatures

Substance	Transition	Actual temperature (°C) (by Mettler)	Observed ternperature (°c) (by Pressure cell)
C-CH_2	Isotropic-Nematic	48.4	46.1
NPOOB	Isotropic-Nematic	66.2	65.8
	Nematic-Srnectic A	60.1	59.3
C-CH_4	Isotropic-Nematic	79.0	77.8
7OPDOB	Isotropic-Nematic	87.6	86.2
	Nematic-Smectic A	84.0	82.7
CBNA	Isotropic-Nematic	104.9	103.7
	Nematic-Smectic A	99.1	97.2
HOAB	Isotropic-Nematic	123.6	122.2
		94.3	91.9
PAA	Isotropic-Nematic	135.0	132.4
PAP	Isotropic-Nematic	165.0	161.9

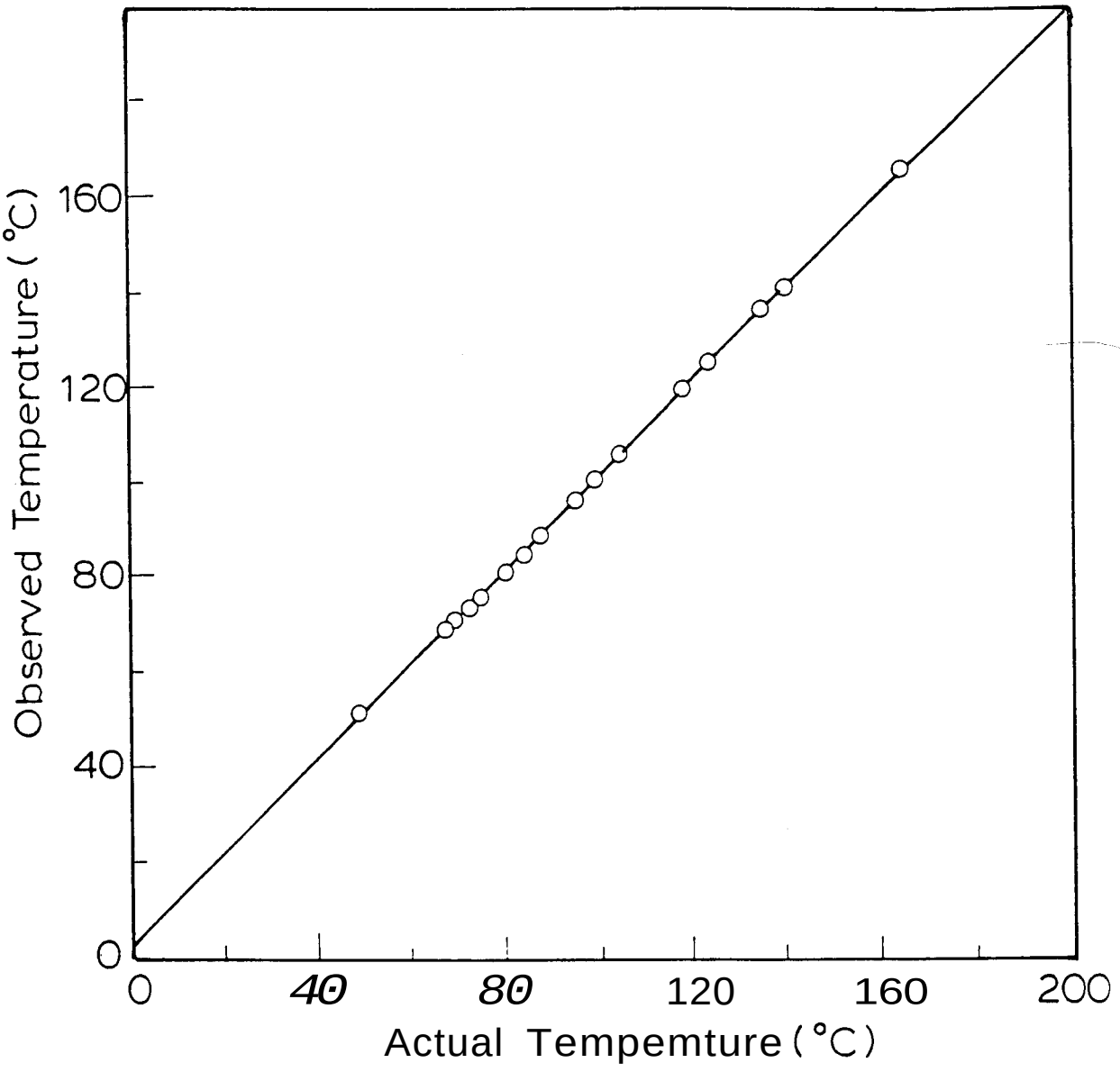

Figure 2.16

Temperature calibration curve of the high pressure cell in the cooling mode using the substances listed in Table 2.4.

Pressure calibration of the cell

In order to ascertain that the pressure experienced by the sample is the same as the line pressure read on the gauge, we conducted calibration experiments using p-azoxyanisole (PAA), perhaps the most widely studied liquid crystal under pressure.[7-16] The nematic-isotropic transition was used for the purpose. The experiments were conducted on both increasing and decreasing pressure cycle and it was found that the transition temperature at any pressure was independent of the pressure cycling. This showed that the sample in the cell was experiencing hydrostatic pressure.

The accuracy of the pressure measurement was ±1.5 bar while the transition temperature were read to an accuracy of ±25 mK or better.

REFERENCES

1 A.J.Leadbetter, J.C.Frost, J.P.Gaughan, G.W.Gray and A. Mosley, J. de Phys., 40, 375 (1979)

2 F. Hardouin, A.M.Levelut, J.J.Benattar and G.Sigaud, Solid State Commun., **33,** 337 (1980)

3 P.E.Cladis and D. Guillon (Private communication)

4 A.N.Kalkura, R.Shashidhar and M.SubramanyaRaj Urs, J. de Phys., 44, 51 (1983)

5 A.N.Kalkura, "High Pressure Optical Studies of Liquid Crystals", Ph. D. Thesis, University of Mysore, 1982.

6 S.Krishna Prasad, "High Pressure Studies of Liquid Crystalline Transitions", Ph. D. Thesis, University of Mysore, 1985.

7 G.A.Hulett, Z. Phys. Chem., **28,** 629 (1899)

8 N.A.Puschin and I.W.Grebenschtschikow, Z. Phys. Chem., 57, 270 (1926)

9 J. Robberecht, Bull. Soc. Chum. Belg., 47, 597 (1938)

10 N.A.Tikhomirova, L.K.Vistin and V.N.Nosov, Sov. Phys.-Crystallogr. (Engl. Trans.), 17, 878 (1973).

11 S. Chandrasekhar, S.Ramaseshan, A.S.Reshamwala, B.K.Sadashiva, R.Shashidhar and V.Surendranath, Proc. Int. Liq. Cryst. Conf., Bangalore, 1973 - Pramana, Suppl. 1, 117 (1975).

12 W. Klement and L.H.Cohen, Mol. Cryst. Liq. Cryst., 27, 359 (1974)

14 W.Spratte and G.M.Schneider, Ber. Bunsenges. Phys. Chem., 80, 886 (1976)

14 B. Deloche, B.Cabane and D. Jerome, Mol. Cryst. Liq. Cryst., 15, 197 (1971)

15 V. Ya. Baskakov, V.K.Semenchenko and N.A.Nedostup, Sov. Phys. Crystallogr. (Engl. Trans.), 19, 112 (1974); V.Ya.Baskakov, V.K.Semenchenko and V.M.Byankin, Sov. Phys. JETP (Engl. Trans.), **39,** 383 (1974).

16 S.M.Stishov, V.A.Ivanov, and V.N.Kachinskii, JETP Lett. (Engl. Trans.), 24, 297 (1977).